Physics of Plasmas

A second order yield-temperature relation for accurate inference of burn-averaged quantities in multi-species plasmas

Cite as: Phys. Plasmas **28**, 022701 (2021); https://doi.org/10.1063/5.0032139
Submitted: 06 October 2020 . Accepted: 08 January 2021 . Published Online: 01 February 2021

N. V. Kabadi, P. J. Adrian, A. Bose, D. T. Casey, J. A. Frenje, M. Gatu Johnson, B. Lahmann, O. M. Mannion, R. D. Petrasso, H. G. Rinderknecht, F. H. Séguin, H. W. Sio, G. D. Sutcliffe, and A. B. Zylstra

Physics of Plasmas ARTICLE scitation.org/journal/php

A second order yield-temperature relation for accurate inference of burn-averaged quantities in multi-species plasmas

Cite as: Phys. Plasmas **28**, 022701 (2021); doi: 10.1063/5.0032139
Submitted: 6 October 2020 · Accepted: 8 January 2021 ·
Published Online: 1 February 2021

N. V. Kabadi,[1,a)] P. J. Adrian,[1] A. Bose,[1] D. T. Casey,[2] J. A. Frenje,[1] M. Gatu Johnson,[1] B. Lahmann,[1] O. M. Mannion,[3] R. D. Petrasso,[1] H. G. Rinderknecht,[3] F. H. Séguin,[1] H. W. Sio,[2] G. D. Sutcliffe,[1] and A. B. Zylstra[2]

AFFILIATIONS

[1]Massachusetts Institute of Technology Plasma Science and Fusion Center, Cambridge, Massachusetts 02139, USA
[2]Lawrence Livermore National Lab, Livermore, California 94550, USA
[3]University of Rochester Laboratory for Laser Energetics, Rochester, New York 14623, USA

[a)]Author to whom correspondence should be addressed: Kabadi@mit.edu

ABSTRACT

Measured yields and ion temperatures inferred from the fusion product energy spectra can be used as metrics for the performance of an ICF implosion. This can be used to infer species separation, thermal decoupling, flows, or other effects that can cause the inferred ion temperatures to deviate from the true underlying thermal temperature and the yield ratio to deviate from the expected value. Direct inference of the impact of these effects on observed temperatures and yields can be difficult to uncover due to the underlying dependence on the shape and time evolution of the temperature and density profiles of the fusing plasma. Due to differences in the temperature dependence of the reactivities, different fusion products are emitted from different regions and times within the implosion. In order to properly account for this, a second-order analytical expression relating the apparent temperatures and yield ratios is developed. This expression can be coupled to models of yield and/or temperature altering effects to infer their burn-averaged impact on an implosion. The second-order expression shows significant improvement over lower-order expressions in synthetic data studies. Demonstrations of its applications to synthetic data coupled with models of ion thermal decoupling and radial flows are presented. In the case of thermal decoupling, both first and second-order expressions show reasonable levels of accuracy. To consistently infer the amplitude of radial flow with a $<10\%$ error, the second-order equation is required.

I. MOTIVATION

The goal of an inertial confinement fusion (ICF) experiment is to couple laser energy to a dense fuel-layer. As this shell converges its kinetic energy, it is coupled to the central hot spot's thermal energy. The density and temperature of the hot spot increase, and fusion burn is initiated.[1] During the period of nuclear emission, there are significant temporal and spatial variations in the hot spot temperature and density profiles. These temporal and spatial profiles dictate the location and time of nuclear emission. Because the reactivities of individual fusion reactions often have different temperature dependencies,[2] burn-averaged nuclear observables from different reactions, like ion temperatures, are weighted to different locations and times. Throughout this paper, this spatial and temporal weighting will be referred to as profile effects. In Fig. 1, this effect is shown for an isobaric heat conduction-limited model of a DT^{3}He-filled implosion. This model will be discussed later in this paper. In this example, all species have identical density and temperature profiles, but it is clear that the DT, DD, and D^{3}He fusion reactions have different spatial weighting due to differences in the shape of their reactivity vs temperature curve. This also results in the different reactions producing different time histories, as can be seen in Fig. 2. The majority of current work using burn-averaged nuclear observables makes comparisons without taking into account the effect of these differences in the emission location and time[3–6] or uses profiles taken from hydrodynamic models or simulations.[7,8] As will be shown in this paper, neglecting temperature profile effects can result in large errors when inferring

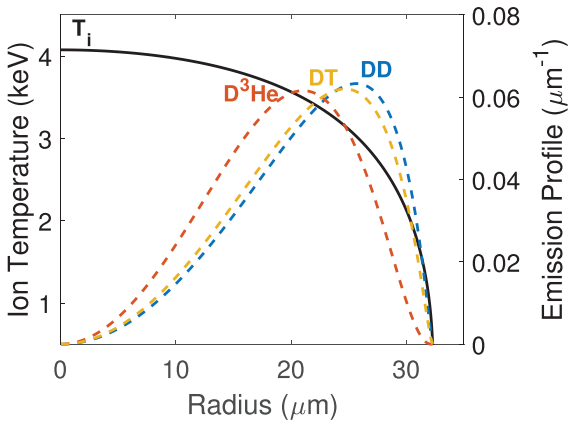

FIG. 1. Plot of the ion temperature vs radius for a heat conduction-limited hotspot model and the resulting fusion emission profiles for DT, DD, and D^3He reactions. The emission profiles are yield normalized so the relative shapes can be compared.

other burn-averaged properties from the measured yields and temperatures. For example, greater than 100% error in inferred radial flow velocity is observed when using a uniform model. To improve this state of affairs, a higher-order relation accounting for temperature variation is necessary.

In Secs. II A–II D, an analytical expression relating measured ion temperatures and yield ratios, accurate to second order in temperature variation, is developed. Density variations will not be accounted for as all nuclear fusion reactions have an identical density dependence. In the case where different species have independent density profiles, this relation would not be applicable. Beyond this limitation, the relation has wide applicability to most multi-species implosion types and even non-ICF fusion plasmas. The model is developed by first expanding the definition of the nuclear fusion yield as a function of temperature. Then, the definition of burn-averaged temperature is expanded.

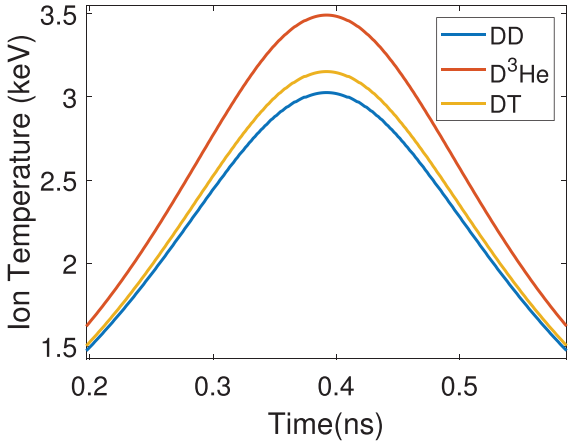

FIG. 2. Plots of time evolution of the emission averaged ion temperatures for DT, DD, and D^3He fusion from an isobaric, adiabatic compression with heat conduction-limited temperature profiles. The peak values and shape of the evolution are clearly different for the different reactions. The peak temperatures for each reaction occur at the same time as the density and temperature maxima occur simultaneously in this model.

Finally, these two equations are combined to develop a second-order expression relating the measured yield ratio and burn-averaged ion temperatures. This second-order expression can be used to check measurements for consistency, or it can be coupled with additional models to make inferences of other physically important parameters. Sections III A–III C show synthetic data studies that serve to validate the expression and show examples of its application to inferring radial flows and ion thermal decoupling.

II. DERIVATION OF A SECOND-ORDER YIELD-TEMPERATURE RELATION

A. Introduction to important terms

Temperatures inferred from the second moment of fusion product energy spectra will be referred to as spectral temperatures,[9,20] T_{sij}. Measured burn-averaged temperatures are, therefore, $\langle T_{sij}\rangle$, where the subscripts indicate the two reacting species and $\langle\rangle$ indicate averaging over the associated fusion burn, both spatially and temporally. The correct temperature to evaluate the fusion reaction's local reactivity can be different from the spectral value and will be referred to as T_{rij}. It is assumed that there exists a relationship between these two temperatures, which is determined by a model parameter, S, and a "background" temperature, T. S could be any fit parameter within the model relating T_{rij} and T_{sij} and is meant to represent a degree of freedom, such as the presence of radial flows or thermal disequilibrium, to name two possibilities. Examples of how to leverage this degree of freedom to infer information about the plasma are included in Sec. III. The physical meaning of the background temperature is unimportant as it will be eliminated from the expressions shortly. The exact form of this relation will be dependent on the specific physics model(s) included. To maintain generality, these will be written as

$$T_{sij} = T_{sij}(S, T),$$
$$T_{rij} = T_{rij}(S, T),$$

where parentheses, (), denote the functional dependence. If there are no effects altering the spectral temperature or reactivity from the thermal value, $T_{rij} = T_{sij}$ and the model parameter S is not necessary. These relations are applied to the reactions of two like species and two unlike species, for example, DT and DD fusion in a DT-filled implosion or D^3He and DD in a D^3He-filled implosion. Assuming that the relations can be inverted, T is eliminated from the different equations and all the relevant temperatures can be written in terms of T_{s11},

$$T_{s12} = T_{s12}(S, T_{s11}),$$
$$T_{r11} = T_{r11}(S, T_{s11}),$$
$$T_{r12} = T_{r12}(S, T_{s11}).$$

It is important to keep in mind that these relations are given by an imposed model, which is why they can be reparameterized in terms of whatever variables are most useful. In this case, choosing to expand about the measured $\langle T_{s11}\rangle$ results in necessary cancelations further down the line.

The eventual goal is to relate the measured yields and temperatures. To do this, the ratio of the reactivities of the two reactions being analyzed is expanded. The expanded form will be inserted into the definitions for yield and burn-averaged temperature. To properly expand about $\langle T_{s11}\rangle$, derivatives need to be taken with respect to T_{s11}. The reactivity ratio, R, is expressed as

$$R = \frac{\langle\sigma v_{12}\rangle(T_{r12})}{\langle\sigma v_{11}\rangle(T_{r11})} = \frac{\langle\sigma v_{12}\rangle(T_{r12}(T_{s11}))}{\langle\sigma v_{11}\rangle(T_{r11}(T_{s11}))} = R(T_{s11}),$$

where the explicit dependence on the model parameter, S, has been dropped for simplicity. Expanding to second order gives

$$R \approx R_o + R'_o[T_{s11} - \langle T_{s11}\rangle] + \frac{1}{2}R''_o[T_{s11} - \langle T_{s11}\rangle]^2, \quad (1)$$

where

$$R_o = R|_{T_{s11}=\langle T_{s11}\rangle},$$
$$R'_o = \frac{\delta R}{\delta T_{s11}}|_{T_{s11}=\langle T_{s11}\rangle},$$
$$R''_o = \frac{\delta^2 R}{\delta T_{s11}^2}|_{T_{s11}=\langle T_{s11}\rangle}.$$

R is a known function, and so R_o, R'_o, and R''_o can be computed. Plots of R and its first and second derivatives for DT and D^3He plasmas are shown in Fig. 3. For this plot, it is assumed that $T_{r11} = T_{r12}$. Due to the extra factor of T_{sij} in the definition of burn-averaged temperature, $\langle T_{sij}\rangle$, another expansion including this factor is needed. The necessary function (P) is constructed as R times the ratio of the spectral temperatures,

$$P(T_{s11}) = R\frac{T_{s12}(T_{s11})}{T_{s11}}.$$

In the case where T_{s11} and T_{s12} are determined entirely by the thermal temperature, $P = R$. Otherwise, P is used to account for differences in the spectral temperatures. P will be used to make a first-order estimate of the plasma ion temperature variance, as will be seen in Sec. II C. For this reason, P is expanded to only first order,

$$P \approx P_o + P'_o[T_{s11} - \langle T_{s11}\rangle], \quad (2)$$

where

$$P_o = P|_{T_{s11}=\langle T_{s11}\rangle},$$
$$P'_o = \frac{\delta P}{\delta T_{s11}}|_{T_{s11}=\langle T_{s11}\rangle}.$$

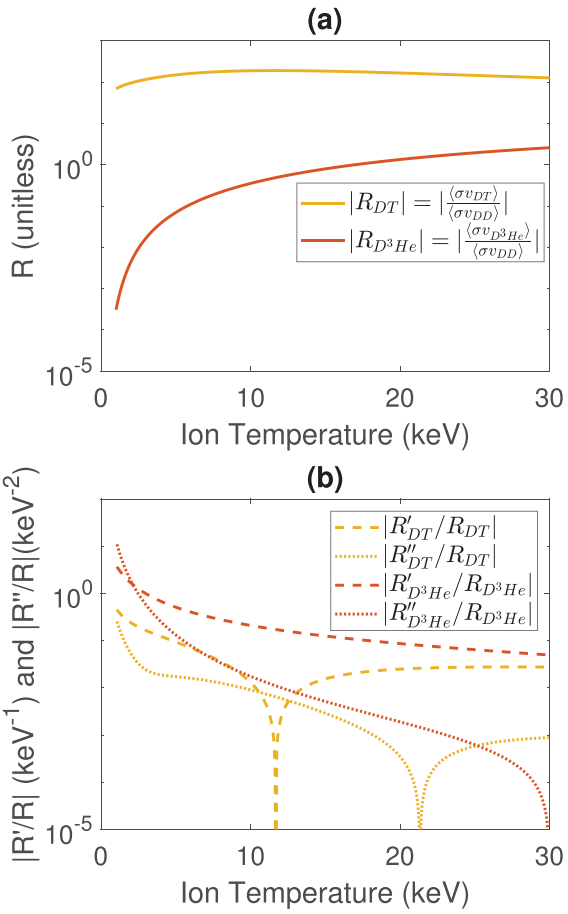

FIG. 3. (a) Plot of the reactivity ratios vs ion temperature for DT and D3He plasmas. (b) Plot of the first and second derivatives of the reactivity ratios, normalized to the value of the ratio at that temperature.

B. Expansion of the yield expression

Starting from the integral expression for the fusion yield of the two unlike reactants, R is inserted and then the expansion from Eq. (1) is used to produce an approximate expression for the yield ratio. In Secs. II C and II D, explicit temperature dependencies will be dropped for clarity. It is assumed that the two species have identical density profiles in space and time up to a constant. If this is not the case, the following relations would not hold and a more complex model allowing for species fraction variation would be necessary. The constant fraction of species i within the fuel is taken to be f_i,

$$\begin{aligned} Y_{12} &= \int n_1 n_2 \langle\sigma v_{12}\rangle dVdt \\ &= f_1 f_2 \int n^2 \langle\sigma v_{12}\rangle dVdt \\ &= f_1 f_2 \int n^2 \langle\sigma v_{11}\rangle R dVdt \\ &\approx f_1 f_2 \int n^2 \langle\sigma v_{11}\rangle \left[R_o + R'_o[T_{s11} - \langle T_{s11}\rangle]\right. \\ &\quad \left. + \frac{1}{2}R''_o[T_{s11} - \langle T_{s11}\rangle]^2\right] dVdt. \end{aligned}$$

Looking at this integral term by term and using the definitions $Y_{11} = \frac{f_1^2}{2}\int n^2\langle\sigma v_{11}\rangle dVdt$ and $\langle T_{s11}\rangle = \frac{f_1^2}{2Y_{11}}\int n^2\langle\sigma v_{11}\rangle T_{s11} dVdt$,

$$f_1 f_2 \int n^2 \langle\sigma v_{11}\rangle R_o dVdt = 2\frac{f_2}{f_1} R_o Y_{11},$$
$$f_1 f_2 \int n^2 \langle\sigma v_{11}\rangle R'_o[T_{s11} - \langle T_{s11}\rangle] dVdt$$
$$= 2\frac{f_2}{f_1} R'_o Y_{11}[\langle T_{s11}\rangle - \langle T_{s11}\rangle] = 0,$$
$$f_1 f_2 \int n^2 \langle\sigma v_{11}\rangle \frac{1}{2}R''_o[T_{s11} - \langle T_{s11}\rangle]^2 dVdt$$
$$= \frac{f_2}{f_1} R''_o Y_{11}\left[\langle T_{s11}^2\rangle - \langle T_{s11}\rangle^2\right].$$

Defining the spectral temperature variance, σ_{11}^2, of the reaction of species 1 with itself as $\langle T_{s11}^2\rangle - \langle T_{s11}\rangle^2$, the expression is simplified to

$$Y_{12} \approx 2\frac{f_2}{f_1} Y_{11}\left[R_o + \frac{1}{2}R_o''\sigma_{11}^2\right].$$

The yield ratio can be written as

$$\frac{Y_{12}}{Y_{11}} \approx 2\frac{f_2}{f_1}\left[R_o + \frac{1}{2}R_o''\sigma_{11}^2\right]. \tag{3}$$

This expression for the yield ratio should be correct to second order in both temporal and spatial temperature variations. The largest issue with this expression alone is that σ_{11}^2 is unknown. It could potentially be estimated from simulations, but this is not ideal. In order to eliminate σ_{11}^2 from this expression, another equation relating it to the measured yield ratio and temperatures is necessary. To develop this, the definition of $\langle T_{s12}\rangle$ is chosen as the starting point.

C. Expansion of the burn-averaged ion temperature expression

The next expression relating σ_{11}^2 to the measured temperatures and yield ratio is derived by starting from the definition of $\langle T_{s12}\rangle$. This time the expansion of P from Eq. (2) will be inserted,

$$\begin{aligned}\langle T_{s12}\rangle &= \frac{f_1 f_2}{Y_{12}}\int n^2\langle\sigma v_{12}\rangle T_{s12} dV dt,\\ &= \frac{f_1 f_2}{Y_{12}}\int n^2\langle\sigma v_{11}\rangle T_{s11} P dV dt\\ &\approx \frac{f_1 f_2}{Y_{12}}\int n^2\langle\sigma v_{11}\rangle T_{s11}\left[P_o + P_o'[T_{s11} - \langle T_{s11}\rangle]\right] dV dt.\end{aligned}$$

Looking at the two terms in the integral separately,

$$\frac{f_1 f_2}{Y_{12}}\int n^2\langle\sigma v_{11}\rangle T_{s11} P_o dV dt = 2\frac{f_2}{f_1}\frac{Y_{11}}{Y_{12}} P_o\langle T_{s11}\rangle,$$

$$\frac{f_1 f_2}{Y_{12}}\int n^2\langle\sigma v_{11}\rangle T_{s11} P_o'[T_{s11} - \langle T_{s11}\rangle] dV dt = 2\frac{f_2}{f_1}\frac{Y_{11}}{Y_{12}} P_o'\sigma_{11}^2.$$

Substituting these back in, it is found that

$$\langle T_{s12}\rangle \approx 2\frac{f_2}{f_1}\frac{Y_{11}}{Y_{12}}\left[P_o\langle T_{s11}\rangle + P_o'\sigma_{11}^2\right].$$

The yield ratio can then be solved for

$$\frac{Y_{12}}{Y_{11}} \approx 2\frac{f_2}{f_1}\frac{1}{\langle T_{s12}\rangle}\left[P_o\langle T_{s11}\rangle + P_o'\sigma_{11}^2\right]. \tag{4}$$

This is a first-order yield temperature relation that also depends on σ_{11}^2. In Sec. II D, Eqs. (3) and (4) will be combined to develop the final second-order yield temperature relation.

D. The final second-order yield-temperature expression

At this point, independent second-order and first-order expressions for the yield ratio have been developed, both of which depend on σ_{11}^2. The value of σ_{11}^2 will be approximated at first order and then inserted into Eq. (3) to achieve the final second-order expression. To approximate the value of σ_{11}^2 at first order, the second-order yield ratio expression, Eq. (3), can be truncated at first order and set equal to the first-order temperature based on Eq. (4),

$$\begin{aligned}R_o &\approx \frac{1}{\langle T_{s12}\rangle}\left[P_o\langle T_{s11}\rangle + P_o'\sigma_{11}^2\right],\\ \sigma_{11}^2 &\approx \frac{R_o\langle T_{s12}\rangle - P_o\langle T_{s11}\rangle}{P_o'}.\end{aligned} \tag{5}$$

In combination with the second-order yield ratio equation, Eq. (3), this completes a second-order analytical expression relating the yield ratio and measured temperatures. This is written explicitly as

$$\frac{Y_{12}}{Y_{11}} \approx 2\frac{f_2}{f_1}\left[R_o + \frac{1}{2}R_o''\frac{R_o\langle T_{s12}\rangle - P_o\langle T_{s11}\rangle}{P_o'}\right]. \tag{6}$$

Although σ_{11}^2 is estimated at first order, it is multiplied by R_o'' in the final expression, which maintains the entire expression as second order. With this general formulation, the model parameter, S, can be iterated to find the value that best matches the measured yield ratio. The exact choice of S and the relations between the different temperatures will depend on the specific model chosen. The inferred value will be accurate to second order in both temporal and spatial temperature variations. As subsequently shown, this expression is valid for temperatures sufficiently far from inflection points in the reactivity ratio and, as previously stated, requires that both species have similar density profiles. Examples demonstrating how to formulate the different components are shown in Secs. III A–III C.

III. SYNTHETIC DATA TESTS OF THE SECOND-ORDER YIELD-TEMPERATURE EXPRESSION

A. Accuracy accounting for temperature profile effects only

As a first test of this second-order expression, (6), it can be applied to synthetic ICF data where the only effect is profile weighting. To produce these synthetic data, an adiabatic, isobaric, and thin-shell compression model is used. In this model, the radial trajectory is fixed entirely by the initial pressure, radius, and implosion velocity. The equation governing the trajectory of a thin shell is

$$M_{shell}\frac{d^2 r}{dt^2} = 4\pi r^2 P,$$

where r is the shell position, M_{shell} is the shell mass, and P is the central pressure. The pressure evolution as a function of shell radius is fixed for an ideal gas by the adiabatic compression assumption to be

$$P \propto V^{-5/3} \propto r^{-5}.$$

Combining these two expressions, the final radial trajectory can be solved for. Imposing initial conditions for pressure (P_o), radius (r_o), and shell velocity (v_o), the shell trajectory is

$$r(t) = \left[r_o^2 + \left[v_o^2 + \frac{4\pi P_o r_o^3}{M_{shell}}\right]t^2 + 2r_o v_o t\right]^{\frac{1}{2}}.$$

The initial conditions were tuned to give physically relevant yields and ion temperatures, and then the initial implosion velocity was incrementally increased in order to vary the synthetic ion temperatures.

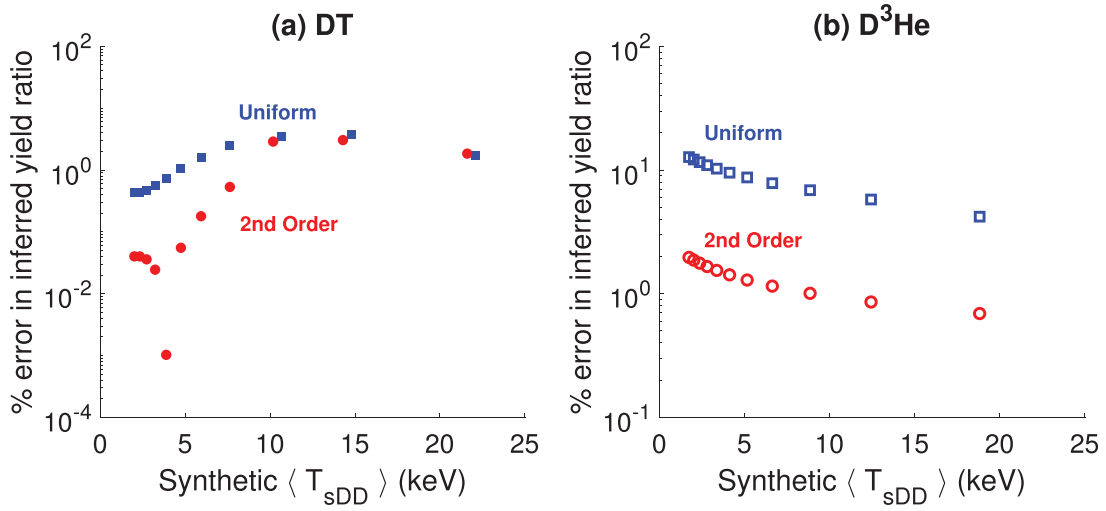

FIG. 4. (a) Plot of the error in the inferred yield ratio for synthetic DT data vs the synthetic burn-averaged DD ion temperature. (b) Plot of the error in the inferred yield ratio for synthetic D^3He data vs the synthetic burn-averaged DD ion temperature. Blue squares are the uniform zeroth-order model, and red circles are the second-order model. Some of the blue squares have been offset to avoid the overlap.

This model imposes temporal variation, but spatial variation is also necessary to properly test the second-order expression. The analytical isobaric heat conduction-limited profiles of Betti *et al.*[10] were used to impose spatial temperature and density profiles. Examples of the temperature radial profile and time history are shown in Figs. 1 and 2. Reactivities were evaluated using the interpolation formulas of Bosch and Hale.[2] Using this model, synthetic yields and spectral temperatures were computed. Based on the synthetic temperatures, the expected yield ratio is computed using Eq. (6) and compared with the correct synthetic value.

In the case of synthetic data, which only include temperature profile weighting, T_{s11} is sufficient to fully define the model and no additional fit parameter (S) is included,

$$\begin{aligned} T_{s12} &= T_{s11}, \\ T_{r11} &= T_{s11}, \\ T_{r12} &= T_{s11}, \\ R = P &= \frac{\langle \sigma v_{12} \rangle (T_{s11})}{\langle \sigma v_{11} \rangle (T_{s11})}. \end{aligned} \tag{7}$$

Together, Eqs. (6) and (7) constitute the second-order model. To check the accuracy, the yield ratio as estimated from the second-order model can be compared with the known yield ratio from the synthetic implosion data. Figure 4 shows the error in the inferred yield ratio from the analytical second-order expression plotted vs the synthetic burn-averaged DD ion temperature. This is done for both 50:50 DT, Fig. 4(a), and 70:30 D^3He fills, Fig. 4(b). For comparison, the results of applying a 0th-order uniform model are also shown.

For the DT case, the second-order model consistently achieves yield ratio errors $<10\%$, which is similar to the typical neutron time-of-flight measurement uncertainties for yields and ion temperatures at the national ignition facility.[11] When the ion temperature is less than 10 keV, the second-order expression shows significant improvement in the accuracy of the inferred yield ratio when compared to uniform. Above 10 keV, there is little to no improvement. This is because the ratio of the DT to DD reactivity has an inflection point at $\approx$12 keV where the first derivative goes to 0. Not only does this make the higher-order correction negligible in comparison to the uniform model, but also it causes a reversal in the ordering of terms such that the second-order term can become dominant in comparison to the first. As a result, the first-order estimate of σ^2_{DD} is no longer valid. This can be seen in Fig. 5 where the error in the inferred σ^2_{DD}, as computed using Eq. (5), is large in the region of this inflection point. This error does not propagate into the estimated yield ratio as the variance is multiplied by R'', which is 100$\times$ smaller than the 0th-order term in this region. The ratio of D^3He to DD reactivity is continually varying throughout the temperature range tested, which is apparent in Fig. 4(b), where the second-order expression consistently provides an

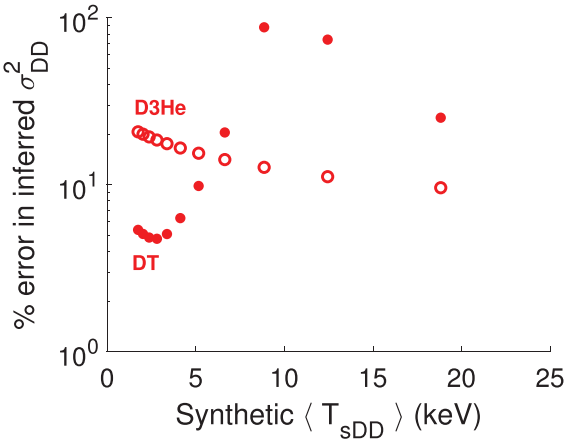

FIG. 5. Error in the inferred DD temperature variance for synthetic DT data (filled points) and D^3He data (open points).

order of magnitude accuracy improvement. This is also seen in Fig. 5 where the error in the inferred σ_{DD}^2 remains low for all the explored temperatures. This exercise serves to verify the accuracy of the second-order expression and demonstrates clear improvement over the uniform model in a temperature range sufficiently far from inflection points in the reactivity ratio. If experimentally measured ion temperatures and yield ratios from an implosion are not consistent with this relation, it would indicate that some effect is impacting the measured ion temperatures or effective reactivities. In Secs. III B and III C, applications of this model to two such effects, radial flows and thermal decoupling, are illustrated.

B. Inference of radial flows

The spectral and reactivity temperatures including the impact of flow broadening can be approximated as[12]

$$T_{s11} = T + 2m_1 S,$$
$$T_{s12} = T + [m_1 + m_2]S,$$
$$T_{r11} = T,$$
$$T_{r12} = T,$$

where the product masses have been approximated as the reactant masses for simplicity and the model parameter S is taken to be the variance of the flow along the line of sight that the spectral measurement is made,

$$S = \langle v_{LOS}^2 \rangle - \langle v_{LOS} \rangle^2,$$
$$v_{LOS} = \vec{v} \cdot \vec{r}_{LOS}.$$

Here, r_{LOS} is the radial vector pointing from the implosion to the detector location and $\langle\rangle$ indicate averaging over the nuclear emission. If the flow variance is assumed to be caused entirely by uniform radial motion, the variance can be related to the radial flow velocity by geometry as[13]

$$S = \frac{1}{3} v_r^2,$$

where v_r is the radial velocity. The temperature relations are reparameterized in terms of T_{s11}, giving

$$T_{s12} = T_{s11} + m_2 S,$$
$$T_{r11} = T_{s11} - 2m_1 S,$$
$$T_{r12} = T_{s11} - 2m_1 S.$$

R and P can then be written as

$$R = \frac{\langle \sigma v_{12} \rangle (T_{s11} - 2m_1 S)}{\langle \sigma v_{11} \rangle (T_{s11} - 2m_1 S)}, \tag{8}$$

$$P = \frac{\langle \sigma v_{12} \rangle (T_{s11} - 2m_1 S)}{\langle \sigma v_{11} \rangle (T_{s11} - 2m_1 S)} \left[1 + \frac{m_2 S}{T_{s11}}\right]. \tag{9}$$

These equations, (8) and (9), combined with the second-order yield ratio equation, (6), complete a model that can be used to infer the flow variance along a given line of sight, which can, in turn, be used to infer the average radial flow velocity. This model can be tested by applying it to synthetic data for which the true burn-averaged flow velocity is known. To do this, the same adiabatic isobaric model with heat conduction-limited profiles is used, but instead of varying the initial conditions, the effective velocity was artificially enhanced when computing the fusion product spectra.

The results of applying the second, first, and zeroth analytical models to the synthetic data are shown in Fig. 6, which shows the error in the inferred velocity vs the true burn-averaged value. The thermal burn-averaged ion temperature, neglecting flows, was ~3 keV in this analysis. This test shows that the second-order model is the most accurate and consistent with errors near or below 10% for all DT data. The first-order and second-order models have more variance in the error and higher, many times unacceptable, error. For both DT and D^3He synthetic data, the error decreases as the imposed flow velocity increases because a larger flow component is more easily distinguished from the background temperature and profile effects. This indicates

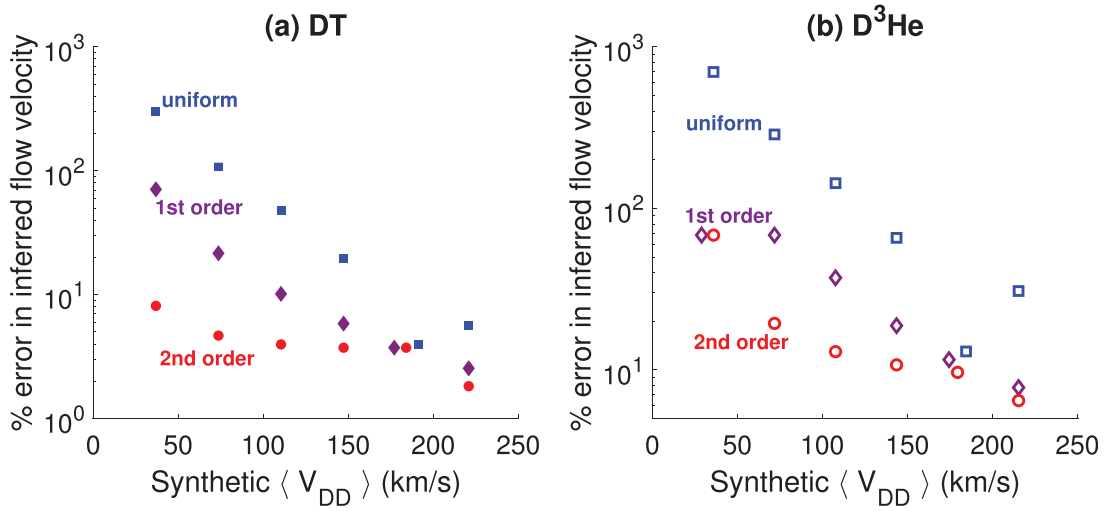

FIG. 6. (a) Plot of the error in the inferred radial flow velocity for synthetic DT data and (b) D^3He data vs the synthetic burn-averaged DD flow velocity. Blue data points are the uniform zeroth-order model, purple the first-order model, and red the second-order model. Some blue and purple data points have been offset to avoid the overlap.

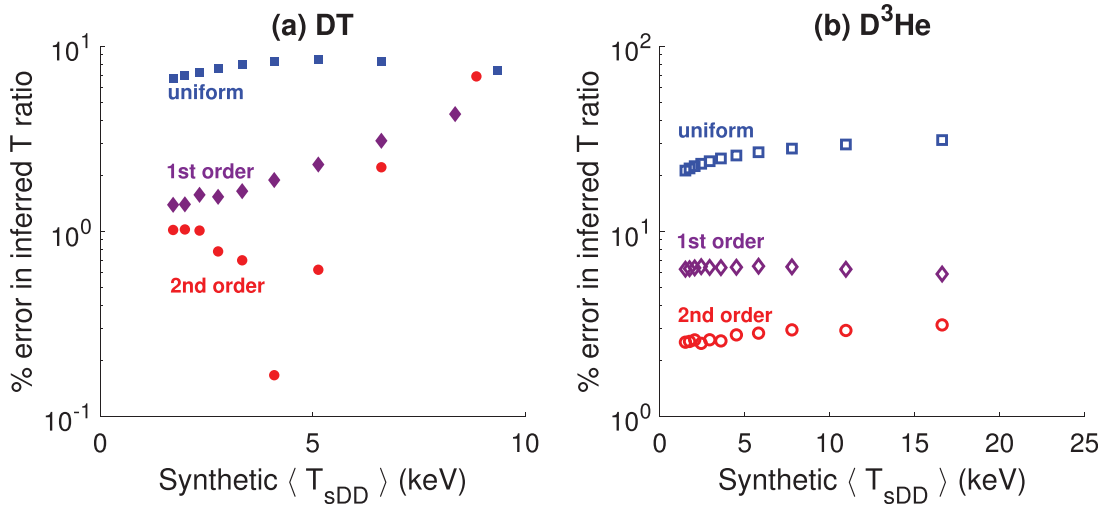

FIG. 7. (a) Plot of the error in the inferred ion species temperature ratio for synthetic DT data and (b) D^3He data vs the synthetic burn-averaged DD ion temperature. Blue squares are the uniform zeroth-order model, purple diamonds are the first-order model, and red circles are the second-order model.

that accurate and consistent inference of the flow variance in a true experiment will require the use of a second-order, or higher, model accounting for temperature profiles.

C. Inference of thermal disequilibrium

Thermal decoupling, in which two ion species have different temperatures, can possibly occur in plasmas that are low density and high temperature, for which the timescale for ion–ion thermal equilibration is long compared to the dynamic timescale of the system. An example of this is the shock convergence phase of ICF implosions. For real experiments in this plasma regime, there will likely be other effects like species separation and reactivity reduction due to loss of high energy ions. These effects could be accounted for with a more complex model but, for simplicity, will be neglected here. For reactions between two ion populations with different temperatures, T_1 and T_2, the effective spectral and reactivity temperature can be written as[14,15]

$$\begin{aligned} T_{s11} &= T_1, \\ T_{s12} &= \frac{m_1 T_1 + m_2 T_2}{m_1 + m_2}, \\ T_{r11} &= T_1, \\ T_{r12} &= \frac{m_2 T_1 + m_1 T_2}{m_1 + m_2}, \end{aligned}$$

where T_1 and T_2 are the individual species temperatures. For this model of thermal decoupling, the parameter S is taken to be the ratio of these two temperatures, $S = \frac{T_2}{T_1}$. Then,

$$\begin{aligned} T_{s12} &= \frac{m_1 + m_2 S}{m_1 + m_2} T_{s11} = A T_{s11}, \\ T_{r11} &= T_{s11}, \\ T_{r12} &= \frac{m_2 + m_1 S}{m_1 + m_2} T_{s11} = B T_{s11}. \end{aligned}$$

R and P can be written as

$$R = \frac{\langle \sigma v_{12} \rangle (B T_{s11})}{\langle \sigma v_{11} \rangle (T_{s11})}, \tag{10}$$

$$P = \frac{\langle \sigma v_{12} \rangle (B T_{s11})}{\langle \sigma v_{11} \rangle (T_{s11})} A. \tag{11}$$

Equations (10) and (11) for R and P, together with the second-order yield ratio equation, (6), form a model for thermal decoupling while taking into account the effect of temperature profile weighting. To test this model, it was applied to synthetic data produced using the same isobaric, adiabatic model with heat conduction-limited density and temperature profiles. In addition, an artificial temperature ratio between the two ion species was applied. To impose spatial and temporal variation, the temperature ratio was taken to have a maximum value given by the mass ratio and vary directly proportional to the absolute temperature in space and time. $\frac{T_2}{T_1}(t,r) = 1 + [\frac{m_2}{m_1} - 1]\frac{T(t,r)}{T_{max}}$. The resulting burn-averaged temperature ratios are ~1.3 for this synthetic dataset. The initial implosion velocity was adjusted to vary the burn-averaged temperature. Figure 7 shows the error in the inferred temperature ratio plotted vs the burn-averaged DDn temperature. For the DT test case, it is seen that up to 7 keV, the first- and second-order models show incremental improvements when compared to the uniform model. The D^3He test case shows more substantial improvements as the reactivity ratio is steeper as a function of temperature, making the higher-order corrections larger. This is apparent from Fig. 7(b) where there is substantial improvement in the inferred ion temperature ratio when going from uniform to higher-order models. Altogether, this demonstrates that the second-order model works well for making inferences of the level of thermal decoupling.

IV. CONCLUSIONS

The second-order yield-temperature relation developed and validated in this paper shows significant improvement over both uniform and first-order models within its region of validity. This formalism

will allow modeling of apparent temperature and/or yield altering effects without the need to either neglect profiles or assume specific profiles. The model is shown to be valid for temperatures that are sufficiently far from inflection points in the reactivity ratio. It was specifically validated for DT-filled implosions with temperatures in the range of 1–7 keV and D^3He-filled implosions with temperatures in the range of 1–20 keV. The exact dynamics and type of implosion are not important as long as both species have similar density profiles. Situations where the two species have independent spatial profiles would require more complex modeling. While this work focused on implosions, the derived model could be applied to a variety of plasmas as long as they are within the given temperature ranges. The expression can be used to improve the analysis of previous datasets and should be used when applicable for future data analysis. Previous results, which used discrepant yield ratios as evidence for species separation, should be revisited.[6,8] Also, experiments using a uniform model to infer reactivities of fusion reactions may need revision. In many experiments, this may not be possible as two temperatures are not always measured and the importance of the correction will depend on the exact reactions being probed. Going forward, the model can be used for inferring the flow variance in ignition relevant DT-filled implosions at Omega and the NIF. This residual kinetic energy has been shown to correlate with implosion performance, making it an important parameter to accurately quantify in experiments.[16–19]

ACKNOWLEDGMENTS

This material is based upon the work supported by the Department of Energy, National Nuclear Security Administration under Award Nos. DE-NA0003868 and DE-NA0003938.

This report was prepared as an account of the work sponsored by an agency of the United States Government. Neither the United States Government nor any agency thereof, nor any of their employees, makes any warranty, express or implied, or assumes any legal liability or responsibility for the accuracy, completeness, or usefulness of any information, apparatus, product, or process disclosed, or represents that its use would not infringe privately owned rights. Reference herein to any specific commercial product, process, or service by trade name, trademark, manufacturer, or otherwise does not necessarily constitute or imply its endorsement, recommendation, or favoring by the United States Government or any agency thereof. The views and opinions of the authors expressed therein do not necessarily state or reflect those of the United States Government or any agency thereof.

DATA AVAILABILITY

The data that support the findings of this study are available from the corresponding author upon reasonable request.

REFERENCES

[1]J. D. Lindl, P. Amendt, R. L. Berger, S. G. Glendinning, S. H. Glenzer, S. W. Haan, R. L. Kauffman, O. L. Landen, and L. J. Suter, "The physics basis for ignition using indirect-drive targets on the National Ignition Facility," Phys. Plasmas **11**, 339–491 (2004).

[2]H.-S. Bosch and G. Hale, "Improved formulas for fusion cross-sections and thermal reactivities," Nucl. Fusion **32**, 611–631 (1992).

[3]D. T. Casey, J. A. Frenje, M. Gatu Johnson, M. J.-E. Manuel, H. G. Rinderknecht, N. Sinenian, F. H. Séguin, C. K. Li, R. D. Petrasso, P. B. Radha, J. A. Delettrez, V. Y. Glebov, D. D. Meyerhofer, T. C. Sangster, D. P. McNabb, P. A. Amendt, R. N. Boyd, J. R. Rygg, H. W. Herrmann, Y. H. Kim, and A. D. Bacher, "Evidence for stratification of deuterium-tritium fuel in inertial confinement fusion implosions," Phys. Rev. Lett. **108**, 075002 (2012).

[4]C. Forrest, P. Radha, J. Knauer, V. Glebov, V. Goncharov, S. Regan, M. J. Rosenberg, T. Sangster, W. Shmayda, C. Stoeckl, and M. G. Johnson, "First measurements of deuterium-tritium and deuterium-deuterium fusion reaction yields in ignition-scalable direct-drive implosions," Phys. Rev. Lett. **118**, 095002 (2017).

[5]H. Sio, J. Frenje, A. Le, S. Atzeni, T. Kwan, M. Gatu Johnson, G. Kagan, C. Stoeckl, C. Li, C. Parker, C. Forrest, V. Glebov, N. Kabadi, A. Bose, H. Rinderknecht, P. Amendt, D. Casey, R. Mancini, W. Taitano, B. Keenan, A. Simakov, L. Chacón, S. Regan, T. Sangster, E. Campbell, F. Seguin, and R. Petrasso, "Observations of multiple nuclear reaction histories and fuel-ion species dynamics in shock-driven inertial confinement fusion implosions," Phys. Rev. Lett. **122**, 035001 (2019).

[6]H. Sio, O. Larroche, S. Atzeni, N. V. Kabadi, J. A. Frenje, M. Gatu Johnson, C. Stoeckl, C. K. Li, C. J. Forrest, V. Glebov, P. J. Adrian, A. Bose, A. Birkel, S. P. Regan, F. H. Seguin, and R. D. Petrasso, "Probing ion species separation and ion thermal decoupling in shock-driven implosions using multiple nuclear reaction histories," Phys. Plasmas **26**, 072703 (2019).

[7]H. W. Herrmann, J. R. Langenbrunner, J. M. Mack, J. H. Cooley, D. C. Wilson, S. C. Evans, T. J. Sedillo, G. A. Kyrala, S. E. Caldwell, C. S. Young, A. Nobile, J. Wermer, S. Paglieri, A. M. McEvoy, Y. Kim, S. H. Batha, C. J. Horsfield, D. Drew, W. Garbett, M. Rubery, V. Y. Glebov, S. Roberts, and J. A. Frenje, "Anomalous yield reduction in direct-drive deuterium/tritium implosions due to H_3e addition," Phys. Plasmas **16**, 056312 (2009).

[8]H. G. Rinderknecht, M. Rosenberg, C. Li, N. Hoffman, G. Kagan, A. Zylstra, H. Sio, J. Frenje, M. Gatu Johnson, F. Séguin, R. Petrasso, P. Amendt, C. Bellei, S. Wilks, J. Delettrez, V. Glebov, C. Stoeckl, T. Sangster, D. Meyerhofer, and A. Nikroo, "Ion thermal decoupling and species separation in shock-driven implosions," Phys. Rev. Lett. **114**, 025001 (2015).

[9]L. Ballabio, J. Källne, and G. Gorini, "Relativistic calculation of fusion product spectra for thermonuclear plasmas," Nucl. Fusion **38**, 1723 (1998).

[10]R. Betti, M. Umansky, V. Lobatchev, V. N. Goncharov, and R. L. McCrory, "Hot-spot dynamics and deceleration-phase Rayleigh–Taylor instability of imploding inertial confinement fusion capsules," Phys. Plasmas **8**, 5257–5267 (2001).

[11]R. Hatarik, D. B. Sayre, J. A. Caggiano, T. Phillips, M. J. Eckart, E. J. Bond, C. Cerjan, G. P. Grim, E. P. Hartouni, J. P. Knauer, J. M. Mcnaney, and D. H. Munro, "Analysis of the neutron time-of-flight spectra from inertial confinement fusion experiments," J. Appl. Phys. **118**, 184502 (2015).

[12]T. J. Murphy, "The effect of turbulent kinetic energy on inferred ion temperature from neutron spectra," Phys. Plasmas **21**, 072701 (2014).

[13]
$$\frac{1}{4\pi R^2}\int_0^{\pi} 2\pi R^2 \sin\theta v_r^2 cos^2\theta d\theta = \frac{1}{3}v_r^2.$$

[14]C. Bellei, H. Rinderknecht, A. Zylstra, M. Rosenberg, H. Sio, C. K. Li, R. Petrasso, S. C. Wilks, and P. A. Amendt, "Species separation and kinetic effects in collisional plasma shocks," Phys. Plasmas **21**, 056310 (2014).

[15]A. Inglebert, B. Canaud, and O. Larroche, "Species separation and modification of neutron diagnostics in inertial-confinement fusion," Europhys. Lett. **107**, 65003 (2014).

[16]P. T. Springer, O. A. Hurricane, J. H. Hammer, R. Betti, D. A. Callahan, E. M. Campbell, D. T. Casey, C. J. Cerjan, D. Cao, E. Dewald, L. Divol, T. Doeppner, M. J. Edwards, J. E. Field, C. Forrest, J. Frenje, J. A. Gaffney, M. Gatu-Johnson, V. Glebov, V. N. Goncharov, G. P. Grim, E. Hartouni, R. Hatarik, D. E. Hinkel, L. B. Hopkins, I. Igumenshchev, P. Knapp, J. P. Knauer, A. L. Kritcher, O. Landen, A. Pak, S. L. Pape, T. Ma, A. G. MacPhee, D. H. Munro, R. C. Nora, P. K. Patel, L. Peterson, P. B. Radha, S. P. Regan, H. Rinderknecht, C. Sangster, B. K. Spears, and C. Stoeckl, "A 3D dynamic model to assess the impacts of low-mode asymmetry, aneurysms and mix-induced radiative loss on capsule performance across inertial confinement fusion platforms," Nucl. Fusion **59**, 032009 (2019).

[17]K. M. Woo, R. Betti, D. Shvarts, A. Bose, D. Patel, R. Yan, P.-Y. Chang, O. M. Mannion, R. Epstein, J. A. Delettrez, M. Charissis, K. S. Anderson, P. B. Radha, A. Shvydky, I. V. Igumenshchev, V. Gopalaswamy, A. R. Christopherson, J.

Sanz, and H. Aluie, "Effects of residual kinetic energy on yield degradation and ion temperature asymmetries in inertial confinement fusion implosions," Phys. Plasmas **25**, 052704 (2018).
[18]R. Shah, B. Haines, F. Wysocki, J. Benage, J. Fooks, V. Glebov, P. Hakel, M. Hoppe, I. Igumenshchev, G. Kagan, R. Mancini, F. Marshall, D. Michel, T. Murphy, M. Schoff, K. Silverstein, C. Stoeckl, and B. Yaakobi, "Systematic fuel cavity asymmetries in directly driven inertial confinement fusion implosions," Phys. Rev. Lett. **118**, 135001 (2017).
[19]M. Gatu Johnson, B. D. Appelbe, J. P. Chittenden, A. Crilly, J. Delettrez, C. Forrest, J. A. Frenje, V. Y. Glebov, W. Grimble, B. M. Haines, I. V. Igumenshchev, R. Janezic, J. P. Knauer, B. Lahmann, F. J. Marshall, T. Michel, F. H. Séguin, C. Stoeckl, C. Walsh, A. B. Zylstra, and R. D. Petrasso, "Impact of imposed mode 2 laser drive asymmetry on inertial confinement fusion implosions," Phys. Plasmas **26**, 012706 (2019).
[20]H. Brysk, "Fusion neutron energies and spectra," Plasma Phys. **15**, 611–617 (1973).